Smectic Surface Structures in the Isotropic Phase of Liquid Crystalline Polymers Studied by X-ray Reflectivity

H. Elben and G. Strobl*

Fakultät für Physik der Universität, 7800 Freiburg, Germany

Received June 17, 1992; Revised Manuscript Received November 12, 1992

ABSTRACT: In an X-ray reflectivity study of thin films of several liquid crystal-side group polymers, boundary layers with a smectic structure were detected in the isotropic phase. They possess a remarkable stability and exist also at larger distances from the clearing point. Reflectivity curves were evaluated in detail by application of the Born approximation on a convenient structure model of the film. A stepwise procedure for the data evaluation is suggested, which enables a separate determination for different groups of model parameters.

Introduction

Polymers with mesogenic side groups constitute a class of materials which combine the properties of polymers with those of liquid crystals.[1,2] Like low molecular weight liquid crystalline compounds, they exhibit fluid anisotropic mesophases which can be oriented by magnetic and electric fields or by surface forces. On the other hand, they possess typical polymer properties. Samples can be oriented by drawing; viscosities are rather high, and structures can be frozen by quenching to temperatures below the glass transition.

The special chemical composition of the liquid crystal (LC)-side group polymers leads to peculiarities in the microscopic structure. Usually there is a tendency to separate the backbone chain sequences from the mesogenic side groups. This is achieved in a natural way in the smectic phase,[3] where the mesogenic groups and backbone chains form individual layers. As indicated by an X-ray structure analysis performed for a LC polysiloxane,[4] a partial separation is retained also in the nematic and even in the isotropic phase. Layers appear to be the dominant structure element through all phases, with long-range ordering in the smectic phase, and local short-range order in the nematic and isotropic phases.

Close to surfaces liquid crystals may exhibit specific structures. They have been observed for low molecular weight liquid crystals at the interface to a solid substrate or at a free surface, in the smectic and nematic mesophases as well as in the isotropic phase. There are boundary layers with smectic order in the nematic phase,[5] or layers with smectic[6] or nematic[7-9] order in the isotropic phase. Effects are generally understood as pretransitional surface ordering phenomena. As observed and discussed in theoretical treatments,[10,11] the thickness of the boundary layer increases on approaching the transition temperature.

In the case of low molecular weight liquid crystals specific surface structures are only observed for temperatures close to the transition point ($T - T_t < 2$ K). As reported in this paper, for LC-side group polymers the respective temperature range can be much larger. Regarding the general tendency to form layers in the bulk of the nematic or the isotropic phase, this does not come as a surprise. One can expect the formation of a boundary layer with a thickness equal to the correlation length of the order fluctuations in the bulk, which apparently shows nonvanishing values also farther away from the transition point.

Measurement of the X-ray reflectivity at surfaces is a convenient technique for detailed studies of surface structures and has gained increasing importance in recent time (compare ref 12 for a review). Measurements are usually performed on thin films, which are placed on a substrate of float glass or silicon. Investigations concern block copolymers, polymer blends, and low molecular weight liquid crystals. For liquid crystals a successive layer-by-layer growth was observed on approaching the clearing point in the isotropic phase.[6,13] We present in the following the results of an X-ray reflection study on a variety of different LC-side group polymers. All compounds possess a smectic phase, either directly below the isotropic phase or separated from the isotropic phase by a nematic phase. In most cases a fully oriented thin film was obtained by spin-coating a polymer solution, followed by evaporation of the solvent. X-ray reflectivity measurements were first used for a characterization of the as-prepared smectic film, which usually was oriented, and then for an analysis of the surface structures at elevated temperatures, in the isotropic and nematic phases. For some of the samples, cooling to temperatures in the smectic phase resulted in a renewed formation of the original oriented structure.

Analysis of reflectivity data requires model assumptions. In the following we shall first introduce a convenient model and discuss the information content of the data. Then the results of our investigations will be presented.

Experimental Section

The compounds under study were synthesized by the group of Professor H. Finkelmann (Institut für Makromolekulare Chemie, Universität Freiburg). Chart I gives the chemical composition and the mesophase behavior of the samples, denoted in the following as S1, S2, S3, and S4. The degree of polymerization was rather low, $P_n \simeq 100$, with a broad distribution ($P_w/P_n \leq 10$). Films were prepared by spin-coating, i.e., by putting a toluene solution of the polymer through a millipore filter on a float-glass slide, and distributing it homogeneously by spinning the sample. Evaporation of the solvent, annealing it in an evacuated chamber, led to the formation of films with a uniform thickness. Film thicknesses were controlled by the polymer concentration in the solution and were typically 20–50 nm. As shown by the X-ray reflection curves, films prepared in this way were usually fully oriented, the smectic layers lying parallel to the substrate surface. X-ray reflectivity measurement experiments were conducted using a modified Kratky camera at a rotating Cu anode as the X-ray source. Figure 1 gives a schematic drawing of the setup. For the necessary rotation of the sample (angle θ) the camera was equipped with a turntable with a stepping motor. The sharp collimation of the X-ray beam effected by the collimation block (K) of the Kratky camera enables measurements down to Bragg angles of $\theta = 0.1° \simeq 2$ mrad. A graphite single crystal (M) was used for monochromatization.

In the given situation the slitlike primary beam can be used without the requirement of applying a desmearing procedure.

* To whom correspondence should be addressed.

0024-9297/93/2226-1013$04.00/0

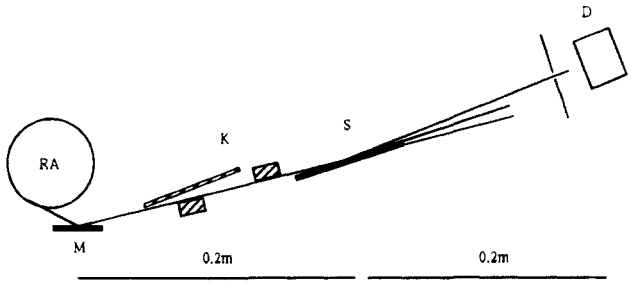

Figure 1. Experimental setup for the X-ray reflection experiments, using a modified Kratky camera (RA, rotating anode; M, monochromator; K, Kratky collimation block; S, sample; D, scintillation counter).

Chart I

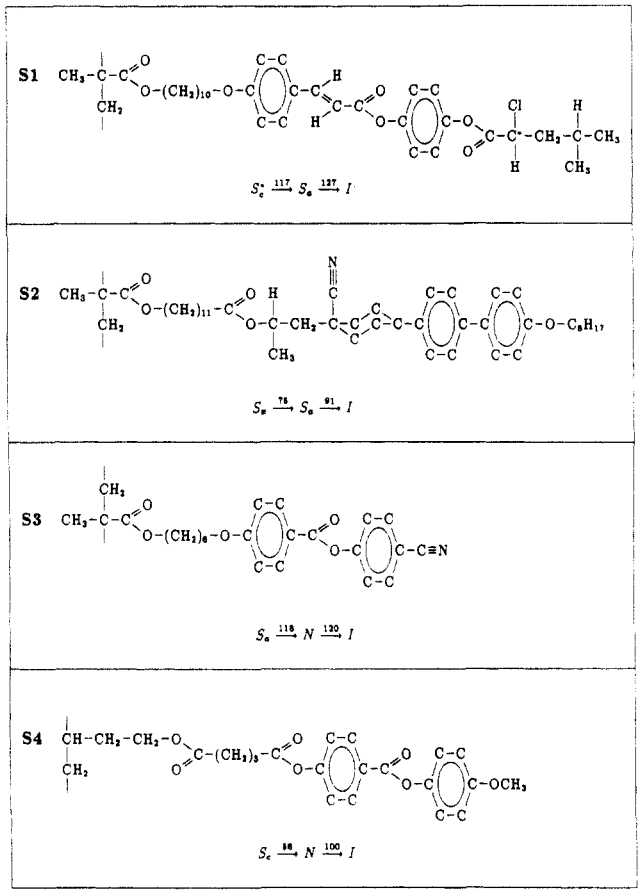

The scattering intensity is concentrated along the q_z axis in reciprocal space, which is oriented parallel to the surface normal. Integration along one of the lateral directions is achieved by the slitlike beam, along the other direction by a scan of the detector (angle θ_d). Reflectivities $R(\theta)$ follow as the ratio of the integral intensities (in θ_d scans) of the specular beam ($\theta_d = 2\theta$) and the primary beam (at $\theta_d = \theta = 0$). Before integrating, the constant (bulk) scattering intensity measured away from the specular beam was subtracted.

A correct positioning of the sample requires the rotation axis of the turntable to be set onto the sample surface and also in the plane of the primary beam. Translation and tilting elements served for this purpose. A first rough adjustment was achieved using a glass slide with a fluorescent coating. This was followed by a refined adjustment for each sample. Samples had a size of 1 × 2 cm. The turntable was equipped with a stage for controlled heating, which enabled temperature-dependent measurements between room temperature and 200 °C.

Principle of X-ray Reflectivity Measurements

The fundamentals of X-ray reflection experiments have been described in the literature (compare e.g. ref 12). We give here only a summary of the main relations.

For an ideal plane surface, reflection and refraction of X-rays are governed by Fresnel's laws. For X-rays the index of refraction becomes smaller than unity:

$$u = 1 - \delta \tag{1}$$

with

$$\delta = r_0 \lambda^2 \rho / 2\pi \tag{2}$$

r_0 is the classical electron radius, λ is wavelength of X-rays, and ρ is electron density (m^{-3}). Usually δ is very small, in the order of $\delta \simeq 10^{-6}$. Absorption is neglected when using eqs 1 and 2.

X-ray beams impinging on a surface are totally reflected for Bragg angles below a critical value:

$$\theta \leq \theta_c \tag{3}$$

with

$$\cos\theta_c = 1 - \delta \rightarrow \theta_c = (2\delta)^{1/2} \tag{4}$$

For $\theta > \theta_c$ the reflectivity $R = S_s/S_p$ (S_s and S_p denote the fluxes of the specular and primary beams) is given by Fresnel's law

$$R_0 = \left[\frac{\theta_c}{\theta + (\theta^2 - \theta_c^2)^{1/2}}\right]^4 \tag{5}$$

$$\approx \frac{\theta_c^4}{16\theta^4} = \frac{r_0^2\lambda^4}{16\pi^2}\rho^2\frac{1}{\theta^4} \quad \text{for } \theta \gg \theta_c \tag{6}$$

or, using the z component of the scattering vector

$$q_z = \frac{4\pi \sin\theta}{\lambda} \tag{7}$$

by

$$R_0 = \frac{q_c^4}{16 q_z^4} \tag{8}$$

with

$$q_c = \frac{4\pi \sin\theta_c}{\lambda} \tag{9}$$

Deviations from an ideal interface structure, i.e., deviations from a steplike profile of the index of refraction, lead to changes in the reflectivity. A simple expression follows in the Born approximation:

$$R = R_0\left|\frac{1}{\rho_\infty}\int \exp(iq_z z)\frac{d\rho}{dz}\,dz\right|^2 \tag{10}$$

Here $\rho(z)$ describes the electron density profile along the surface normal, where ρ changes from $\rho = 0$ (air) to $\rho = \rho_\infty$, the bulk value. Equation 10 is also the equation which follows for the kinematic approximation, which is normally applied in X-ray structure determinations, for the case of the scattering by a simple planar object. The Born (or kinematic) approximation is valid, as long as multiple scattering can be neglected. This is certainly possible for all θ's with $R \leq 10^{-3}$, and is not correct for angles close to θ_c.

There exist also exact formulas for R, which hold for all θ's;[12] however, the Born approximation is much more transparent in a consideration of the effects of different model parameters. We therefore used only eq 10, and restricted the data evaluation to θ's with $R \leq 10^{-3}$.

Structure Model

The structure model assumed in the evaluation of the reflectivity data obtained for the thin films under study is shown in Figure 2. Reflection occurs at the free surface

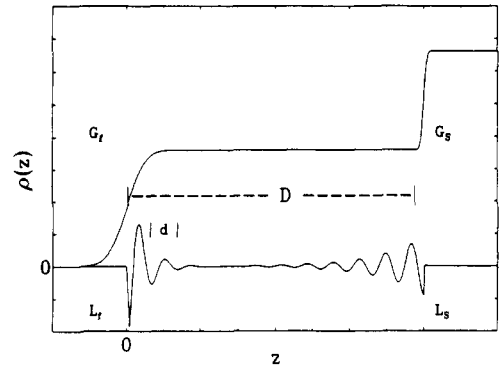

Figure 2. Structure model for a thin film with smectic boundary layers, the different parameters being indicated.

and the polymer–substrate interface. We expect, under appropriate conditions, formation of smectic boundary layers with finite thickness. Both interfaces show a certain roughness, as it is always the case for liquids and glasses. For this model the structure amplitude

$$A(q_z) = \int \exp(iq_z z)\,\frac{d\rho}{dz}\,dz \tag{11}$$

can be represented as a sum of four contributions:

$$A(q_z) = \rho_p G_f + \rho_p L_f + \exp(iq_z D)[(\rho_s - \rho_p)G_s + \rho_p L_s] \tag{12}$$

D gives the film thickness, and ρ_p denotes the electron density of the polymer and ρ_s that of the substrate. G_f and L_f describe the profile at the free surface, for convenience in an additive form. G_f is related to the roughness:

$$G_f = \int \exp(iq_z\Delta z)\frac{1}{(2\pi\sigma_f)^{1/2}}\exp\left(-\frac{(\Delta z)^2}{2\sigma_f^2}\right)d\Delta z$$

$$= \exp(-(\sigma_f^2 q_z^2/2)) \tag{13}$$

Here the roughness is described as resulting from a Gaussian distribution of the displacements at the surface, as they may arise from capillary waves. The width of the transition region is given by σ_f.

For the finite boundary layer with smectic structure we assume a profile

$$\Delta\rho_f(z) = \rho_p\alpha_f \exp(-(\Delta z/\xi_f))\cos(q_0\Delta z - \phi_f) \quad \text{for } \Delta z \geq 0 \tag{14}$$

and

$$\Delta\rho(z) = 0 \quad \text{for } \Delta z < 0$$

Here q_0 is related to the period d of the smectic structure:

$$q_0 = 2\pi/d \tag{15}$$

ξ_f specifies the thickness of the boundary layer; ϕ_f fixes the phase of the smectic density wave and determines which part of the polymer (backbone chain or mesogenic group) is preferentially located at the surface; α_f is the smectic order parameter. L_f is the associated structure amplitude

$$L_f = \frac{1}{\rho_p}\int_{-\infty}^{\infty}\exp(iq_z\Delta z)\,\frac{d\Delta\rho_f}{dz}\,dz$$

which can be transformed, using an integration by parts, into

$$L_f = -iq_z\frac{1}{\rho_p}\int_{-\infty}^{\infty}\exp(iq_z\Delta z)\,\Delta\rho_f\,dz \tag{16}$$

Calculation of the integral eq 16 is straightforward and

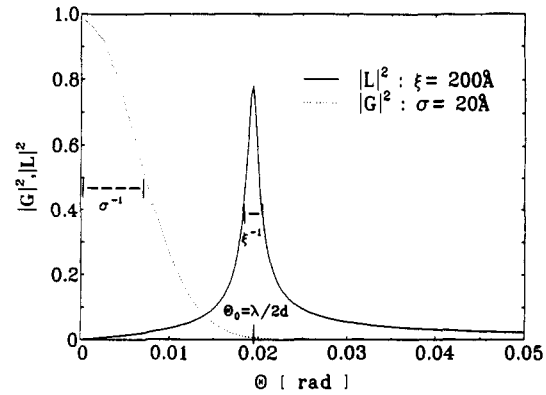

Figure 3. Structure factors associated with the roughened surface ($|G|^2$) and a smectic boundary layer ($|L|^2$).

gives

$$L_f = q_z\xi_f\alpha_f/2\left[\frac{\exp(-i\phi_f)}{(q_z + q_0)\xi_f + i} + \frac{\exp(i\phi_f)}{(q_z - q_0)\xi_f + i}\right] \tag{17}$$

The analogous expressions for the contributions of the polymer–substrate interface are

$$G_s = \exp(-(\sigma_s^2 q_z^2/2)) \tag{18}$$

$$\Delta\rho_s = \rho_p\alpha_s \exp(\Delta z/\xi_s)\cos(-q_0\Delta z - \phi_s) \quad \text{for } \Delta z < 0 \tag{19}$$

$$\Delta\rho_s = 0 \quad \text{for } \Delta z > 0$$

$$L_s = q_z\xi_s\alpha_s/2\left[\frac{\exp(i\phi_s)}{(q_z + q_0)\xi_s - i} + \frac{\exp(-i\phi_s)}{(q_z - q_0)\xi_s - i}\right] \tag{20}$$

Here σ_s characterizes the roughness of this interface, $\Delta\rho_s$ describes the profile of the smectic boundary layer attached to the substrate, and L_s is the associated structure amplitude.

For illustration Figure 3 presents typical forms of G and L (plotting the respective structure factors $|G|^2$ and $|L|^2$). As expected, L shows a peak at $q_z = q_0$.

It is interesting to consider the effect of the model parameters σ and ϕ on the structure factor of one of the surfaces, say the free surface:

$$|A_f|^2 = |\rho_p G_f + \rho_p L_f|^2 \tag{21}$$

Figure 4 shows the result of model calculations, varying ϕ (top) or σ (bottom). One notes a pronounced change with ϕ.

For the purpose of a quantitative evaluation of the reflectivity data eqs 5 and 10–12 were combined to give

$$R(\theta)\theta^4 = R_0\theta^4(1/\rho_s^2)|\rho_p G_f + \rho_p L_f + \exp(iq_z D)[(\rho_s - \rho_p)G_s + \rho_p L_s]|^2 \tag{22}$$

Reflectivity data were evaluated by a least-squares fit on the basis of eq 22, using the Levenberg–Marquard algorithm.

Data Evaluation

Since the model includes quite a few unknown parameters

$$\sigma_f, \alpha_f, \xi_f, \phi_f, \sigma_s, \alpha_s, \xi_s, \phi_s, q_0, D$$

it is important to check at first by qualitative considerations whether they can really be determined by the data fitting. In fact, some of them affect $R(\theta)$ in a specific way, essentially independent of the others, but this is not the case for all parameters. Insight is provided if eq 22 is written in the form

$$R(\theta)\theta^4 = R_0\theta^4(1/\rho_s^2)(P_1 + P_2 + P_3) \tag{23}$$

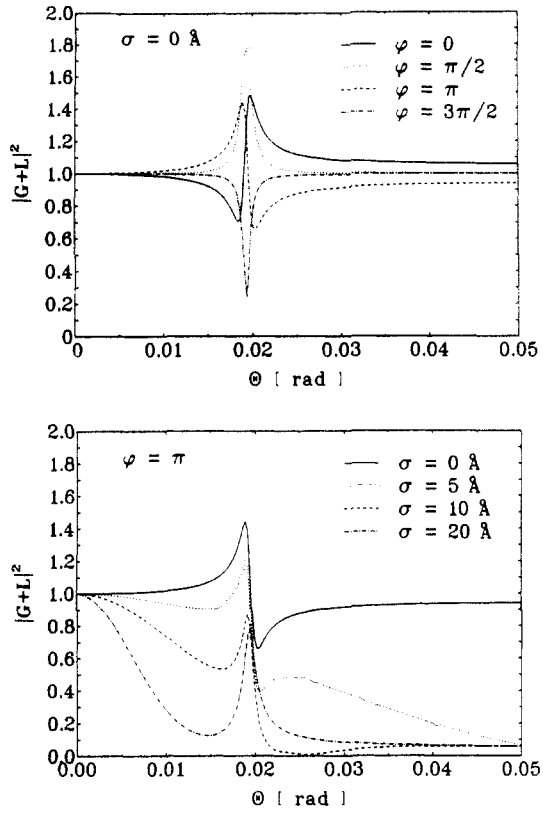

Figure 4. Structure factor associated with one interface ($|L + G|^2$). Effect of a variation of the phase ϕ of the smectic density wave (top) and the roughness parameter σ (bottom).

with

$$P_1 = \rho_p^2 G_f^2 + (\rho_s - \rho_p)^2 G_s^2$$

$$P_2 = 2\mathrm{Re}[\rho_p^2 G_f L_f^* + (\rho_s - \rho_p)\rho_p G_s L_s^*] + \rho_p^2 |L_f|^2 + \rho_p^2 |L_s|^2$$

$$P_3 = 2\mathrm{Re}(\exp(iqD) A_f^* A_s)$$

The first part, $P_1(\theta)$, describes the scattering of two independent rough surfaces. P_1 decreases continuously with increasing θ, like two superposed Debye–Waller functions. $P_2(\theta)$ is the modification introduced by the formation of boundary layers at both interfaces, resulting in changes as they are indicated in Figure 3.

The sum $P_1 + P_2$ describes the scattering by a thick film. For a thin film of constant thickness interference between the two interfaces comes into play. The effect is described by $P_3(\theta)$. $P_3(\theta)$ leads to fluctuations around $P_1 + P_2$, the "Kiessig fringes" with a periodicity of $\Delta q_z = 2\pi/D$.

Data evaluation becomes transparent if the reflectivity curve can be subdivided into the contributions P_1, P_2, and P_3. For the majority of practical cases this was possible, at least approximately: averaging over $\Delta q_z \simeq 2\pi/D$ removes the Kiessig fringes, thus giving $P_1 + P_2$; the difference between the measured and the averaged curve corresponds to P_3; since P_2 gives an essential contribution only around $q_z \simeq q_0$, adjustment of the averaged data omitting this range gives P_1.

Now the information content can be judged. Fitting P_1 gives σ_f and σ_s (θ_c, ρ_p, and ρ_s are usually known). For the samples under study, we always observed a large roughness at the free surface:

$$\sigma_f \approx 15\text{–}20 \text{ Å}$$

The values found for σ_s corresponded to the roughness of an uncoated glass slide:

$$\sigma_s = 3\text{–}5 \text{ Å}$$

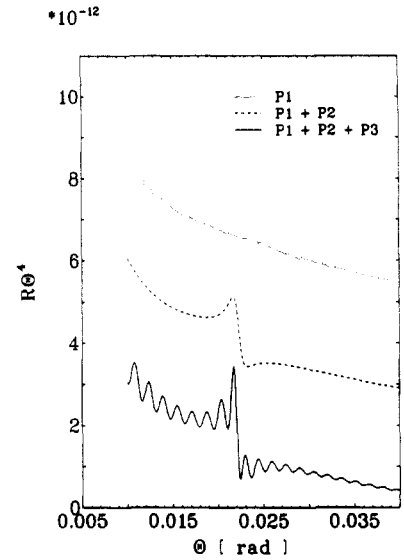

Figure 5. Decomposition of a reflectivity curve ($R\theta^4$ versus θ) typical for a thin film with smectic boundary layers into different contributions.

The half-widths Δq of P_2 and of the envelope of P_3 give the boundary layer thickness, $\Delta q \simeq \xi_f^{-1}$ and ξ_s^{-1}. Separation of ξ_f and ξ_s appears more difficult. In favorable cases P_3 is dominated by the contribution $L_f^* G_s$ ($L_s^* G_f \approx 0$ due to the high roughness σ_f). Then the half-width of P_3 indicates ξ_f. The phase ϕ_s clearly shows up in the form of P_2; ϕ_f normally cannot be determined ($G_f L_f^* \approx 0$; compare Figure 2). With regard to the smectic order parameters α_s and α_f, the situation is similar as for ξ_s and ξ_f: P_2 gives an average value; the separation can be difficult. Precise values are usually obtained for the film thickness D and the smectic layer periodicity $d = 2\pi/q_0$. They follow from the periodicity of the Kiessig fringes and the location of the center of P_2.

Figure 5 gives as an illustration a numerical example, showing the effects of the different contributions P_1, P_2, and P_3 to $R(\theta)$. The calculation refers to the structure shown in Figure 2 with $D = 500$ Å, $d = 35$ Å, $\rho_p = 3.6 \times 10^{23}$ cm^{-3}, and $\rho_s = 6.4 \times 10^{23}$ cm^{-3}.

Results

Figure 6 presents the reflectivity curves measured for *sample S1* during a successive heating and cooling. Here, and also in the following cases, data evaluation was restricted to scattering angles $\theta \geq 0.008$, omitting the range near θ_c, where the Born approximation would not be valid. The qualitative structural features show up directly in the curves. The as-prepared film obviously is fully oriented. As is known from optical microscopy, a S_c^* phase occurs at room temperature. After a transition at 117 °C the S_a phase is stable. The reflectivity curve measured at 119 °C shows that the orientation of the film is retained; the smectic phase disappears at the clearing point (T_c = 127 °C). However, as demonstrated by the appearance of the reflectivity curve at 131 °C, there are smectic boundary layers. Cooling to 124 and 25 °C certainly results in a transition back to the S_a and the S_c^* phases, but the original uniform orientation of the smectic layers in the film does not come back.

The measured curves could be reproduced by the model. The agreement between the experimental data and the model representations (continuous lines) is satisfactory. The model parameters derived from the fit are given in

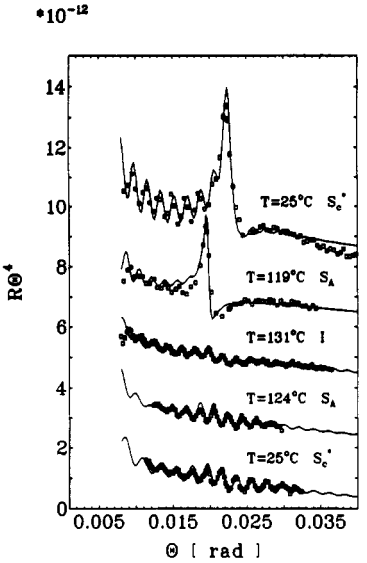

Figure 6. Sample S1. Reflectivity curves measured in the different phases during a heating–cooling cycle (curves are displaced by 2.0×10^{-12}, the lowest curve being in the original position).

Table I
Sample S1: Structure Parameters Derived from the Evaluation of the Reflectivity Curves[a]

T (°C)	phase	σ_f (Å)	σ_s (Å)	D (Å)	d (Å)	ξ (Å)	ϕ_s	ϕ_f	α
25	S_c*	≥15	3	380	30.6	≤380	3.3	3.1	0.12
119	S_a	≥15	3	380	35.1	≤380	3.3	3.1	0.05
131	I	≥15	3	380	33	60	4.0	0.5	0.03
(25	S_c*	≥15	3	380	32	60	3.5	1.0	0.03)

[a] ξ and α are average values of the two interfaces. The data given for S_c* after the heating–cooling cycle are put in parantheses, because they are affected by the loss in orientation.

Table I. As explained above, the parameters differ in their level of confidence. The value obtained for ξ for the as-prepared film, $\xi \lesssim D$, provides evidence for a complete, uniform orientation of the smectic layers. The phase $\phi_s \approx \pi$ indicates that the backbone chains are preferentially attached on the glass surface. There is clear evidence for the occurrence of smectic boundary layers in the isotropic phase. The boundary layers comprise about two smectic layers per interface. Through all temperature steps the roughnesses σ_f and σ_s remain unchanged.

As it was observed in temperature-dependent measurements between room temperature and the clearing point, the smectic period d increases continuously within the range of phase S_c*, from d = 30.6 Å at 25 °C up to d = 35 Å at the transition to phase S_a. The transition $S_c^* \rightarrow S_a$ possesses essentially a second-order character.

Figure 7 shows reflectivity curves obtained within the isotropic phase at different temperatures between 127 and 138 °C. The general appearance suggests a continuous decrease in the thickness of the boundary layers, which exist up to the highest reached temperature. Table II gives the results of the data evaluation.

Results obtained for *sample S2* are presented in Figure 8. This compound possesses also an S_a phase below the isotropic melt (T_t = 91 °C). The observations are similar to those on sample S1: spin-casting produces fully oriented films; there exist smectic boundary layers in the isotropic phase, which appear to be rather stable; cooling back to S_a does not reproduce the original oriented structure. Evaluation of the data yielded the parameter values given in Table III. The continuous curves in Figure 8 give the corresponding representations, which agree well with the measurements.

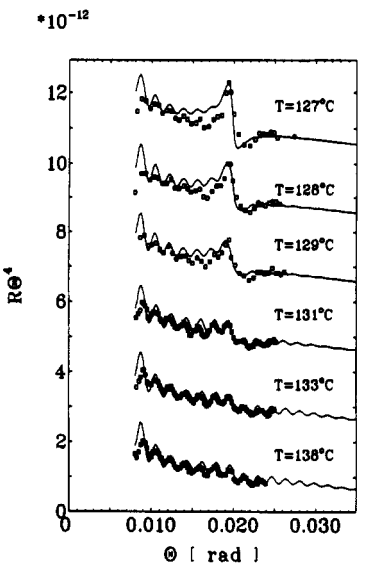

Figure 7. Sample S1. Reflectivity curves measured in the isotropic phase during heating (displacements by 2.0×10^{-12}, lowest curve in original position).

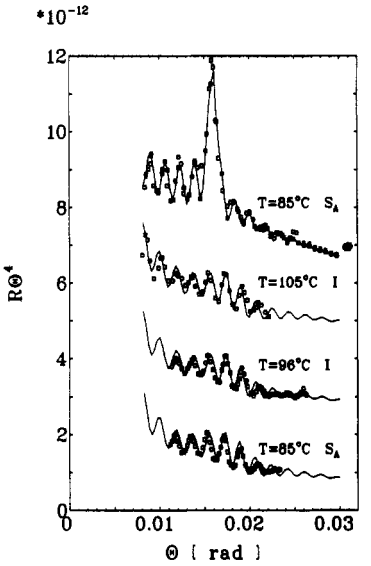

Figure 8. Sample S2. Reflectivity curves measured in the smectic and the isotropic phase (85 °C → 105 °C → 96 °C → 85 °C) (displacements by 2.0×10^{-12}, lowest curve not shifted).

Table II
Sample S1, Isotropic Phase: Thickness and Density Fluctuation Amplitude of the Smectic Boundary Layer and Dependence on Temperature

T (°C)	127	129	131	133	138
ξ (Å)	120	90	60	55	55
$\alpha \times 10^{-2}$	3.5	3.2	3.2	2.8	2.8

Table III
Sample S2: Structure Parameters in the Smectic and the Isotropic Phases, As Derived from the Adjustment of the Reflectivity Data to the Model

T (°C)	phase	σ_f (Å)	σ_s (Å)	D (Å)	d (Å)	ξ (Å)	ϕ_s	ϕ_f	α
85	S_a	20	3.0	390	44	170	1.9	2.0	0.09
105	I	20	3.0	390	38	45	3.3	2.0	0.036

Sample 3 shows in addition to the smectic phase a nematic phase, which is stable in a narrow range of 2° below the clearing point. Figure 9 presents reflectivity curves measured for an as-prepared film, the film at high temperatures in the isotropic phase, and the film after cooling back to the S_a phase (90 °C). In view of the curves one notes that the original film is only partially oriented, there exists a smectic boundary layer in the isotropic phase,

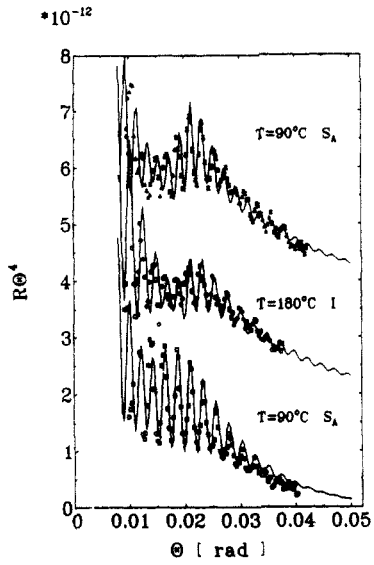

Figure 9. Sample S3. Reflectivity curves measured at 90 °C (S_A) and in the isotropic phase at 180 °C (displacements by 2.0 × 10^{-12}, lowest curve not shifted).

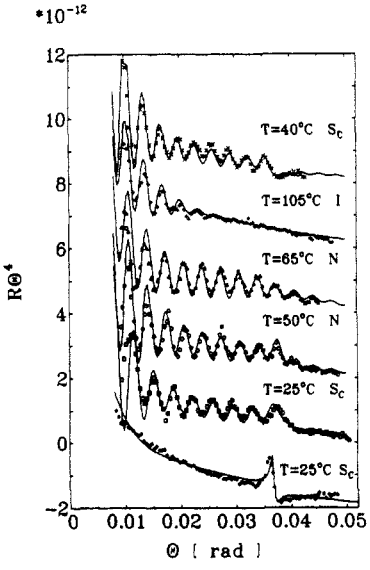

Figure 10. Sample S4. Reflectivity curves measured during a cycle $S_c \rightarrow I \rightarrow N \rightarrow S_c$ for a thin layer, and for a thick layer (D > 2000 Å) at room temperature (curve at the bottom). Curves displaced by 2.0 × 10^{-12}, with the second curve from below in the original position.

even 60 °C above the clearing point, and cooling back from the melt results in an orientation, which is higher than that of the as-prepared film.

The curve fitting yielded the following parameters for the boundary layers at 180 °C: d = 35 Å, $\xi_s \approx \xi_f$ = 35 Å, ϕ_s = 2.0, ϕ_f = 4.9, and D = 280 Å. The evaluation of the data of the S_A film at 90 °C gives only apparent values (ξ = 40 Å), which just demonstrates that the orientation is incomplete. The surprising fact for this sample is the unusual stability of the boundary layer in the isotropic phase.

It is interesting to compare the properties of the samples S1, S2, and S3, which all possess a smectic phase immediately below or beginning a few degrees below the clearing point, with a compound which shows a broad nematic range between the isotropic phase and the smectic phase. *Sample S4* has this property (T_{cn} = 58 °C, T_{ni} = 100 °C). Figure 10 presents reflectivity curves measured in the three phases. In contrast to the other samples, here no boundary layers show up in the isotropic phase ($R(\theta)$ is flat around q_0). In the nematic phase the boundary layer formation is quite pronounced and reversible. Figure 10 shows in addition the reflectivity curve measured for a thick film (D > 2000 Å) at room temperature after a heating–cooling cycle (25 °C → 110 °C → 25 °C). The shape of the reflection at $q_0 = 2\pi/18$ Å^{-1} corresponds to the structure factors $|G + L|^2$ shown in Figure 4 and is therefore indicative for an orientation of the smectic layers in a finite region above the substrate surface. The fit yielded as an estimate for the thickness of the oriented part a value $\xi \approx 360$ Å, corresponding to 20 oriented smectic layers.

The adjusted curves shown in the figure correspond to the following parameters: D = 210 Å, d = 18 Å, σ_f = 15 Å, σ_s = 3 Å (all curves), ξ = 35 and 50 Å at 65 and 50 °C, and ϕ_s = 4.0 and 3.0 at 65 and 50 °C. Films in the smectic phase show only a low degree of orientation.

In conclusion, our studies of LC-side group polymers indicate a strong tendency for the formation of smectic boundary layers in the isotropic phase. They show up if the smectic phase follows in direct sequence to the isotropic phase, or if the existence range of an interfering nematic phase is only small. In contrast to low molecular weight liquid crystals smectic boundary structures were also found at larger distances from the clearing point. They possess a remarkable stability. A thickness increase is observed on approaching the clearing point. Boundary layer formation is discussed in the literature in terms of two different processes, "complete wetting" and "critical adsorption".[10,11,14] Regarding the general tendency of LC-side group polymers to retain a short-ranged layer structure even in the bulk, it is probable that the observed effects are related to critical adsorption. The boundary layer thickness then would correspond to the bulk correlation length. Our experiments did not enable whether there is in addition a complete wetting close to the clearing point to be checked. This would require a sharp phase transition, which is usually not given for LC polymers.

Acknowledgment. This work was supported by a grant of the Deutsche Forschungsgemeinschaft (Sonderforschungsbereich 60 "Funktion durch Organisation in makromolekularen Systemen"). We are also grateful for the support provided by Dr. Otto Röhm, Gedächtnisstiftung.

References and Notes

(1) McArdle, C. B., Ed. *Side Chain Liquid Crystal Polymers*; Blackie: London, 1989.
(2) Finkelmann, H. In *Liquid Crystallinity in Polymers*; Ciferri, A., Ed.; VCH Publishers: New York, 1991.
(3) Stozelecki, L.; Liebert, L. *Bull. Soc. Chim.* **1973**, 597.
(4) Hotz, W.; Strobl, G. *Colloid Polym. Sci.* **1989**, *267*, 889.
(5) Pershau, P. S.; Braslov, A.; Weiss, A. H.; Als-Nielsen, J. *Phys. Rev. A* **1987**, *35*, 4800.
(6) Ocko, B. M.; Braslov, A.; Pershau, P. S.; Als-Nielsen, J.; Deutsch, M. *Phys. Rev. Lett.* **1986**, *57*, 94.
(7) Miyano, K. *Phys. Rev. Lett.* **1979**, *43*, 51.
(8) Chen, W.; Martinez-Mirarde, L. J.; Hsiung, H.; Shen, Y. R. *Phys. Rev. Lett.* **1989**, *62*, 1860.
(9) Immerschitt, S.; Koch, T.; Stille, W.; Strobl, G. *J. Chem. Phys.* **1992**, *96*, 6249.
(10) Allender, D. W.; Henderson, G. L.; Johnson, D. L. *Phys. Rev. A* **1981**, *24*, 1086.
(11) Telo da Gama, M. M. *Mol. Phys.* **1984**, *52*, 585.
(12) Russell, T. P. *Mater. Sci. Rep.* **1990**, *5*, 171.
(13) Ocko, B. M. *Phys. Rev. Lett.* **1990**, *64*, 2160.
(14) Lipowski, R.; Sullivan, D. E. *Phys. Rev. Lett.* **1988**, *60*, 242.